

## Influence of rotation on pulsar emission

R. M. C. Thomas and R. T. Gangadhara  
*Indian Institute of Astrophysics, Bangalore - 560034, India*  
*mathew@iiap.res.in, ganga@iiap.res.in*

---

We analyze the motion of charged particles in rotating pulsar magnetosphere using the equation of motion, which was proposed earlier. We consider the projected magnetic field lines onto a 2D plane perpendicular to the rotation axis, and derive the particle trajectory valid over a radial distance of about 10% of the light cylinder radius. The motive behind considering this model is to elucidate some of the effects of rotation on pulsar profiles. For example, the asymmetry in the observed pulse shapes can be explained by considering the aberration-retardation effects. The single sense circular polarization that has been observed in many pulsars, might be due to the relative orientation of sight line with respect to the plane of particle trajectory.

---

### 1. Introduction

It is difficult to understand fully the emission process in pulsars based on models developed with some simplifying assumptions. Out of several emission mechanisms, curvature emission can be surmised to be the most probable emission mechanism [1-3]. Coherent emission by bunches of particles has been postulated to explain the high brightness temperature observed in pulsars e.g., [3-5]. The polarization observations such as the polarization angle swing favors the curvature radiation. It has been considered as a natural emission process for pulsars, though there are unresolved problems like the bunch formation, orthogonal polarization modes etc e.g., [6-8]. In order to study closely the curvature emission mechanism the influence of rotation has to be properly understood. Machabeli & Rogava [9] have considered the idealized case of particle acceleration where particles move freely along an infinitely long, rigidly rotating straight tube, and derived an expression for the trajectory of a particle. Gangadhara & Lesch [10] have proposed a model for the particle acceleration in rotating magnetosphere in the context of AGN. Reiger & Mannheim [11] have also discussed the particle acceleration along the rotating straight magnetic field lines in AGN, by assuming angular velocity of the particles is same as that of AGN.

Gold [12] was the first one to propose a pulsar emission mechanism based on rotation. Many authors have built upon this model but found it difficult to explain the interpulses e.g., [1]. Blaskiewicz et al. [13] have studied the effects of corotation velocity and Hibschman & Arons [14] have extended their work to include the first order effects because of the phase shifts in polarization angle sweeps due to polar cap currents. Later, Peyman & Gangadhara [15] have improvised the model of Blaskiewicz et al. [13] and analyzed the effect of rotation on the morphology of pulsar profiles and polarization.

Gangadhara [16] has derived the equation of motion of a charged particle in pulsar magnetosphere. He has assumed straight field lines projected on to a 2 dimensional (2D) plane placed perpendicular to the rotation axis. The magnetic Lorentz force acts as a constraining force and drags the plasma along the field lines. Because of the inclination of magnetic axis relative to the rotation axis, corotating plasma tends to rotate with an angular velocity less than that of pulsar on some field lines. We consider the same 2D geometry and analyze the dynamics of a charged particle. We solve the equation of motion, of a charged particle in pulsar magnetosphere, as derived in [16]. We approximate that the field lines close to the magnetic axis are straight lines.

In super strong magnetic fields particles almost stay on the same field lines all along their trajectories because of negligible drift velocity and very small Larmour radius of gyration. Single particle emission is considered in this model and the collective effects are ignored. We take into consideration of the non-uniform angular velocity of particles, which can be less than the pulsar angular velocity on some field lines which are inclined with respect to the meridional plane. Since the particle trajectories are found to be curved, we estimate the curvature emission and analyze the effects of rotation on the radiation characteristics. In sections 2 and 3, we solve the equation of motion of a relativistic charged particle and find its trajectory. In section 4 we estimate the Stokes parameters and plot with respect to different parameters.

## 2. Equation of motion: solution

We solve the equation of motion derived in [16] and find an analytical solution for  $r(t)$ , radial position of the particle as a function of time. We assume that the dipolar magnetic field lines are projected onto a plane perpendicular to the rotation axis, and consider an inertial Cartesian coordinate system as shown in Fig. 1, where the 'z' axis is parallel to the rotation axis ( $\hat{\Omega}$ ) of pulsar. The projected magnetic axis on the x-y plane coincides with the x-axis at time  $t = 0$ . The equation of motion for a charged particle accelerated along a rotating magnetic field line is given by [16],

$$\frac{d}{dt} \left( m \frac{dr}{dt} \right) = m \Omega^* r, \quad (1)$$

where  $m = m_0 \gamma$  is the relativistic mass,  $\gamma$  the Lorentz factor,  $m_0$  rest mass,  $\Omega^*$  the angular velocity and  $r$  the radial position of a particle.

Let  $V_r = dr/dt$  and  $V_\phi = r\Omega^*$  be the components of particle velocity, then

$$\vec{\beta} = \frac{1}{c} (V_r \hat{e}_r + V_\phi \hat{e}_\phi), \quad (2)$$

where  $c$  is the speed of light.

Consider a particle injected at the point B onto a magnetic field line which is inclined by an angle  $\phi_p$  with respect to the x-axis. Let  $d_0 = OB$  be the distance between B and the rotation axis. The effective angular velocity [16] of a particle is given by

$$\begin{aligned} \Omega^* &= \Omega \left[ \frac{r^2 - d_0^2 \cos^2 \theta_0 - d_0 \sin \theta_0 \sqrt{r^2 - d_0^2 \cos^2 \theta_0}}{r (\sqrt{r^2 - d_0^2 \cos^2 \theta_0} - d_0 \sin \theta_0)} \right] \\ &= \Omega \sqrt{1 - \frac{b^2}{r^2}}, \end{aligned} \quad (3)$$

where  $\Omega$  is the angular velocity of pulsar,  $b = d_0 \cos \theta_0$  and  $\theta_0 = (\pi/2) - \phi_p$  is the angle between the field line tangent and  $\hat{e}_\phi$  at B. Using the relation for  $\Omega^*$ , we can write  $\gamma$  as

$$\gamma = \left[ 1 + D^2 - \left( \frac{1}{c} \frac{dr}{dt} \right)^2 - \left( \frac{r\Omega}{c} \right)^2 \right]^{-1/2}, \quad (4)$$

where  $D = \Omega d_0 \cos \theta_0 / c$ . Thus, using the expression for  $\gamma$ , we rewrite Eq. (1):

$$\gamma \frac{d^2 r}{dt^2} + \frac{d\gamma}{dt} \frac{dr}{dt} = \Omega^2 \left( 1 - \frac{b^2}{r^2} \right) \gamma r. \quad (5)$$

By multiplying Eq. (5) with  $r/(\gamma c^2)$ , and defining a dimensionless variable

$$s = \frac{\Omega}{c} \frac{r}{\sqrt{1+D^2}}, \quad (6)$$

we rewrite Eq. (5) as

$$s \frac{d^2 s}{dt^2} + \frac{[2s^2 - D^2/(1+D^2)]}{1-s^2} \left(\frac{ds}{dt}\right)^2 - s^2 \Omega^2 + \Omega^2 \frac{D^2}{1+D^2} = 0. \quad (7)$$

Since  $\theta_0$  is close to  $\pi/2$  for the field lines, which are close to the  $x$ -axis, we find  $D^2 \ll s^2$  for  $d_0 < r$ . Therefore, we reduce Eq. (7) by dropping the terms containing  $D^2/1+D^2$ , and obtain

$$\frac{d^2 s}{dt^2} + \frac{2s}{1-s^2} \left(\frac{ds}{dt}\right)^2 - s \Omega^2 = 0. \quad (8)$$

We solve Eq. (8) and using the expression for  $s$  as given by Eq. (6), we find the radial position of

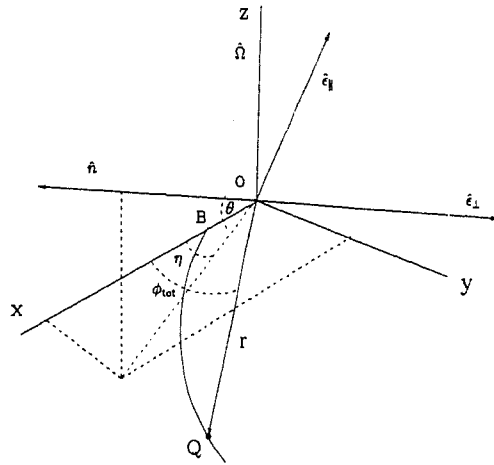


Figure 1: The coordinate system in which the particle motion is considered. The curve BQ represents the particle trajectory in the  $x$ - $y$  plane.

the particle:

$$r = \frac{c\sqrt{1+D^2}}{\Omega} \text{cn}(\lambda - \Omega t). \quad (9)$$

The radial position of the particle according to Eq. (9) as a function of time is plotted in Fig. 2, where we see that the particle position increases with time and reaches a maximum at the distance of light cylinder radius  $r_L = Pc/2\pi$ , where  $P$  is the pulsar period. Next, the particle returns back to origin, due to the reversal of the centrifugal force. This type of oscillatory motion of a particle in an infinitely long, straight and rigidly rotating tube has been discussed in [9].

Though we have extended the calculation of  $r$  of a single particle all the way up to light cylinder, it may not be realistic in the case of plasma motion. Near the light cylinder, plasma inertia causes

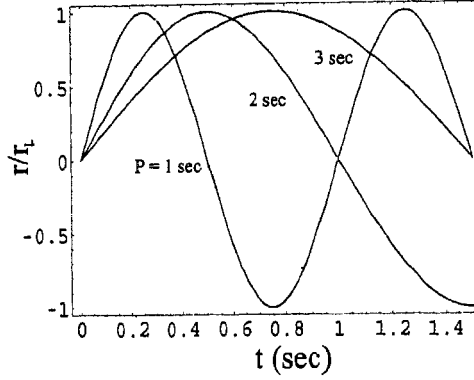


Figure 2: Radial position of the particle as a function of time for  $\gamma_0 = 100$ ,  $d_0 = 10^6$  cm and  $\theta_0 = 90^\circ$ .

the field lines to sweep back and break down of the rigid body motion. The Lorentz factor of a particle, which follows from Eqs. (4), (6) and (8), is given by

$$\gamma = \frac{1}{k\sqrt{(1+D^2)\text{sn}^2(\lambda - \Omega t)}} \quad (10)$$

### 3. Particle trajectory and radius of curvature

In Fig. 3 we consider a particle moving along the field line BQ. The point A represents the particle injection point at time  $t = 0$  that is at a distance  $d_0$  from the rotation axis. The particle co-ordinates can be defined as

$$(x, y) = r(t) (\cos \phi_{\text{tot}}, \sin \phi_{\text{tot}}), \quad (11)$$

where  $\phi_{\text{tot}}$  is the angle between the radial vector to the particle and the  $x$ -axis. From on Fig. 3, we define

$$\phi_{\text{tot}}(t) = \Omega t \pm \phi'(t), \quad (12)$$

where

$$\phi'(t) = \cos^{-1} \left( \cos \phi_p \sqrt{1 - \frac{d_0^2}{r^2} \sin^2 \phi_p} + \frac{d_0}{r} \sin^2 \phi_p \right) \quad (13)$$

For  $d_0 \ll r$ , we find

$$|\phi'(t)| \simeq |\phi_p| \quad (14)$$

The  $\pm$  signs in Eq. (12) correspond to the signs of the angle  $\phi_p$ . In Fig. 4 we have plotted the trajectories of the particles moving along different magnetic field lines, which are marked with  $\phi_p$ . It shows that the trajectories are curved in the direction of rotation of the pulsar. The particles moving in those trajectories are accelerated, and hence they emit curvature radiation. The curvature radii of those trajectories slightly differ from one another, as the particle angular  $\Omega^*$  is different for each field line.

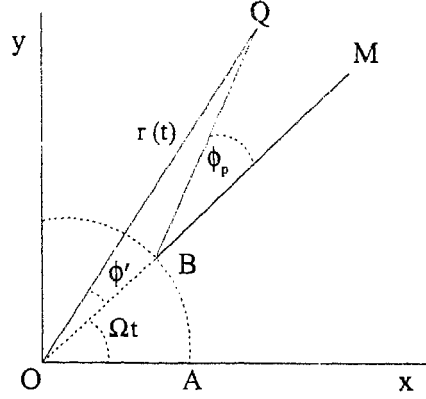


Figure 3: The geometry of motion of a particle along a rotating field line BQ. The angles are  $\angle XOM = \Omega t$ ,  $\angle MBQ = \phi_p$  and  $\angle MOQ = \phi'$ ; and the radius  $OA=OB=d_0$ .

To derive the curvature radii of the particle trajectory, we approximate  $\text{cn}(\lambda - \Omega t)$  and  $r(t)$  using the formalism given by Pearson [17]:

$$\text{cn}(z, k) = \cos z + \frac{k^2}{4}(z - \sin z \cos z) \sin z + O(k^4). \quad (15)$$

In the limit of  $t \ll 1$  and  $k \ll 1$ , the series expansion of  $r(t)$  is given by

$$r(t) = a_0 + a_1 t + a_2 t^2 + a_3 t^3 + a_4 t^4 \dots \quad (16)$$

where  $a_0, a_1, a_2, a_3, a_4 \dots$  are the expansion coefficients.

For  $v_0 \approx c$ , Eq. (12) implies  $k \approx 0$ , therefore, we find  $\lambda = \pi/2$  and  $\text{sn } z = \sin z$ . Thus, we have

$$r(t) \approx \frac{c \sqrt{1+D^2}}{\Omega} \sin(\Omega t). \quad (17)$$

Using the expression for  $r(t)$  and Eqs. (11) and (14), we find the curvature radius of particle trajectory:

$$\begin{aligned} \rho &= \frac{[(dx/dt)^2 + (dy/dt)^2]^{3/2}}{(dx/dt)(d^2y/dt^2) - (dy/dt)(d^2x/dt^2)} \\ &\approx \frac{1}{2} r_L \sqrt{1+D^2} \end{aligned} \quad (18)$$

It shows that the curvature of particle trajectory is approximately  $r_L/2$  for  $\theta_0 = \pi/2$ . However, for other values of  $\theta_0$ ,  $\rho$  becomes slightly larger than  $r_L/2$ . Note that these values are comparable with the curvature radii of dipolar field lines in the emission region given by Gangadhara [18]. The particles are assumed to follow the dipole field lines. The curvature induced by rotation in the particle trajectory for the conal emission components is comparable to the radius of curvature,  $\approx r_L/2$ . The remarkable point is that for the particles accelerated along the field lines very close to the magnetic axis, the inherent radius of curvature of the field lines will be much larger than the radius of curvature induced because of rotation.

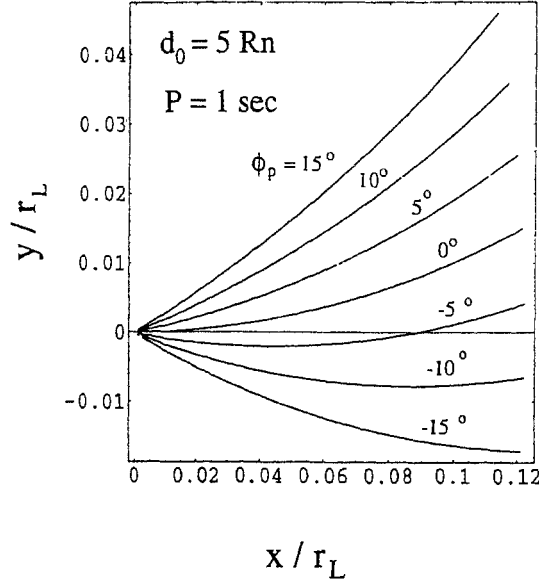


Figure 4: Particle trajectories during the time interval  $0 \leq t \leq 0.02$  sec in laboratory frame. The corresponding field lines lie with in the range  $-15^\circ \leq \phi_p \leq 15^\circ$ , at an interval of  $5^\circ$ . Assumed neutron star radius  $R_n = 10$  Km.

#### 4. Polarization of radiation: Stokes parameters

We derive the Stokes parameters for the radiation emitted by particles accelerated along the rotating field lines. The radiation electric field is given by [7, 19]

$$\mathbf{E}(\omega) = C_f \int_{-\infty}^{+\infty} \hat{n} \times (\hat{n} \times \vec{\beta}) \exp\{i\omega(t - \hat{n} \cdot \vec{r}/c)\} dt, \quad (19)$$

where  $C_f = -i\omega q e^{i\omega S_0/c} / \sqrt{2\pi} S_0 c$ ,  $S_0$  is the distance from the origin to observer,  $\omega$  the radiation frequency and  $\hat{n}$  the sight line. We shall express  $\hat{n} \times (\hat{n} \times \vec{\beta})$  (see, Appendix-A) and the argument of exponential as series expansions in time  $t$  to solve the integral. Consider the sight line  $\hat{n}$  that makes an angle  $\theta$  with the 2D plane, and  $\eta$  with the  $x$ -axis:

$$\hat{n} = (\cos \theta \cos \eta, \cos \theta \sin \eta, \sin \theta). \quad (20)$$

To describe the polarization state of emitted radiation, we define orthogonal unit vectors (see, Fig. 1):

$$\hat{e}_{\parallel} = (-\sin \theta \cos \eta, -\sin \theta \sin \eta, \cos \theta), \quad (21)$$

$$\hat{e}_{\perp} = (-\sin \eta, \cos \eta, 0). \quad (22)$$

The unit vectors  $(\hat{n}, \hat{e}_{\parallel}, \hat{e}_{\perp})$  form an orthogonal triad:

$$\hat{n} \times \hat{e}_{\perp} = \hat{e}_{\parallel}. \quad (23)$$

Let  $t_0$  be the time at which  $\vec{\beta}$  aligns with  $\hat{n}$ , and the observer receives radiation. We transform the time variable  $t$  to  $t + t_0$  such that  $\Omega t_0$  stands for an initial phase. Thus, we find

$$r(t + t_0) = a'_0 + a'_1 t + a'_2 t^2 + a'_3 t^3 + a'_4 t^4 \dots \quad (24)$$

based on Eqs. (15) and (16). The expansion coefficients  $a'_0, a'_1, a'_2, a'_3, a'_4 \dots$  are same as those  $a_0, a_1, a_2, \dots$  except  $\lambda$  replaced by  $\lambda - \Omega t_0$ .

Using Eqs. (9) and (11), we find the series expansion of the exponential argument and keep the terms up to the order of  $t^3$ :

$$\begin{aligned} \omega \left[ (t + t_0) - \frac{\hat{n} \cdot \vec{r}}{c} \right] &= \omega \left[ t + t_0 - \frac{r}{c} \cos \theta (\cos \eta \cos \phi_{\text{tot}} + \sin \eta \sin \phi_{\text{tot}}) \right], \\ &= N_0 + N_1 t + N_2 t^2 + N_3 t^3 \dots \end{aligned} \quad (25)$$

The series expansion of exponential argument is converging, and it is quite obvious from Eqs. (9) and (15). In the limit of  $k \approx 0$ , the series expansion of  $r$  behaves like the trigonometric sin function. Since the angular width of emission beam is  $\approx 2/\gamma$ , the time taken by the particle to cross the angular width of the order of emission beam is  $\approx 2\rho/c\gamma$ . Thus the truncation of higher order terms introduce a negligible error in our calculations. Since we intend to reduce the integral in Eq. (19) to a known form, we limit the series expansion terms up to the order of  $t^3$ .

Using the transformation given by Buschauer & Benford [20], we find the electric field components (see, Appendix-B):

$$E_{\parallel} = \frac{1}{c} (V_{\parallel 0} B_0 + V_{\parallel 1} B_1 + V_{\parallel 2} B_2) C_f e^{iN_0} \sin \theta, \quad (26)$$

$$E_{\perp} = \frac{1}{c} (V_{\perp 0} B_0 + V_{\perp 1} B_1 + V_{\perp 2} B_2) C_f e^{iN_0} \quad (27)$$

Now, we define the Stokes parameters:

$$\begin{aligned} I &= E_{\parallel} E_{\parallel}^* + E_{\perp} E_{\perp}^*, \\ Q &= E_{\parallel} E_{\parallel}^* - E_{\perp} E_{\perp}^*, \\ U &= 2\Re(E_{\parallel}^* E_{\perp}), \\ V &= 2\Im(E_{\parallel}^* E_{\perp}). \end{aligned} \quad (28)$$

The linear polarization is given by

$$L = \sqrt{Q^2 + U^2}. \quad (29)$$

#### 4.1 Stokes parameters of radiation emitted by many particles

We consider a set of field lines on the 2D plane, and estimate the total emission by particles accelerated along them. During pulsar rotation, the sight line stays at a particular  $\theta$  with respect to the 2D plane. Since the emission from each particle is relativistically beamed in the direction of velocity  $\vec{\beta}$ , the observer tends to receive the radiation from all those particles, for which  $\vec{\beta}$  falls within the angular width of  $\pm 1/\gamma$  with respect to  $\hat{n}$ .

First we estimate the Stokes parameters of the radiation emitted by a single particle at the instant  $t_0 \leq t_{\text{max}}$ . The instant  $t_0$  is the time at which  $\hat{n} \cdot \vec{\beta} = 1$  for a given initial  $\phi_p$ . As the rotation progresses, new  $t_0$  is computed for the advanced rotation phase by again solving  $\hat{n} \cdot \vec{\beta} = 1$ , and

computed the Stokes parameters. This procedure is continued till  $t_0 \approx t_{max}$ , where  $t_{max}$  is the time at which the particle goes out of radio emission zone ( $d_0 \leq r \leq 3 \times 10^3$  Km). Since the radiation is emitted over a range of  $r$ , due to the aberration and retardation, the radiation beam gets shifted to the leading side of the pulse. The role of retardation and aberration phase shifts has been discussed by e.g., Phillips [21] and Gangadhara & Gupta [22].

In order to compute the total Stokes parameters with respect to the rotation phase, we sort the Stokes parameters due to single particles into groups of phase bins and add them. In the following steps, we give the details of the procedure:

1. Fixed the observer's sight line at a specific  $\theta$  with respect to the 2D plane.
2. Selected a set of field lines in the range of  $-5^\circ \leq \phi_p \leq 5^\circ$  with a successive line spacing of  $0.1^\circ$ .
3. Solved  $\hat{n} \cdot \hat{\beta} = 1$  to find  $t_0$  at the point of emission on the trajectory corresponding to each field line, and estimated the Stokes parameters at those points.
4. The retardation phase shift  $\Omega(t_{max} - t_0)$  is subtracted from  $\eta$  assigned for each of the emission beam, and estimated the effective rotation phase.
5. Next, the sight line is rotated by  $0.1^\circ$  to a new phase, and repeated the procedure (1-4) over the range of  $-12^\circ \leq \eta \leq 12^\circ$ .
6. Finally, the array of Stokes parameters are sorted into groups of phase bins, and added to get the total pulse profile.

In Fig. 5, we have given the total Stokes parameters computed from the emissions by many particles as functions of rotation phase. In panel (a) we have plotted the profile that is obtained when the sight line lies in the 2D plane, and panel (b) for the case when the sight line is inclined by  $-0.05^\circ$ . The profiles indicate that the peak emissions are shifted to the earlier phase as a consequence of the aberration-retardation effect.

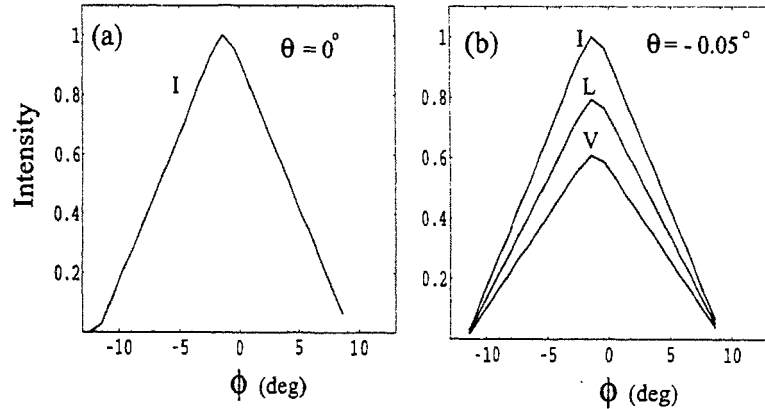


Figure 5: The simulated profiles: panel (a) for  $\theta = 0^\circ$  and panel (b) for  $\theta = -0.05^\circ$ . The parameter  $\phi$  is the rotation phase. Used  $\gamma_0 = 100$  and  $d_0 = 10$  Km.

## 5. Discussion

Since our aim is to understand the rotation effects on particle dynamics and pulse profile, we consider the single particle emission, and leave the collective plasma emissions to latter works. Our region

of interest extends from a few stellar radii to a radial distance well within the light cylinder. In this region the radio emission is expected to occur and the bead-on-wire approximation holds. Our model is more relevant for the cases where the inclination angle  $\alpha$  of the magnetic axis relative to rotation axis is large enough. In such cases, the projected field lines may be approximated to be straight lines over a significant radial distance. We have derived an expression for the radial position of a particle (Eq. 9), which shows an oscillatory behavior, as shown in Fig. 2.

Gangadhara [16] has shown that the particle angular velocity cannot be same as the field line angular velocity if the magnetic axis is inclined with respect to the rotation axis. We considered this effect in our treatment of particle motion, and found the particle trajectories and their curvature radii vary with field line orientation.

Since the magnetic field is very strong drift velocity becomes very small. So, the particles are assumed to follow the same set of field lines all along their trajectories. In the case of single particle dynamics, magnetic field dominates, and hence the rigid body motion may be extended all the way up to the light cylinder. The oscillatory motion that our solution predicts, can not be achieved in a real physical situation like pulsars because of distortion of magnetic field lines due to rotation of the pulsar in the regions close to the light cylinder. So, the particle which reaches the vicinity of the light cylinder can not come back, but can escape from the magnetosphere as a pulsar wind.

We find the radius of curvature of particle trajectory is approximately  $r_L/2$ , which is comparable to the actual radius of curvature of dipolar field lines [18]. So, we believe the curvature emission due to the rotational motion of particles should be comparable to the actual curvature emission in corotating frame.

In a later work, Rogava et al. [23] have showed that if a particle freely moves along a tube with an arbitrary curvature, the centrifugal force does not reverse always. They have showed that the particles move in the tube with a variable angular velocity. This supports our result that the particles angular velocity on some field lines differs from that of pulsar. That is the particles moving along the field lines with  $\phi_p = 0$  rotate with the angular velocity which is same as the pulsar angular velocity. But those moving along other field lines, for which  $\phi_p \neq 0$ , rotate with the angular velocity which is smaller than the pulsar angular velocity.

By taking into account of aberration-retardation, we have reproduced a simulated pulse profile (Fig. 5) by adding the radiation emitted by particles accelerated on a set of field lines. The sign of  $\phi$  has been flipped to match with the phase sign convention followed in pulsar profiles. The roughness in the curves of Fig. 5 are due to the increments of  $0.1^\circ$  in  $\phi_p$  and  $\eta$ . The choice was made due to the limitation in computing time. However, the smoother profiles can always be generated by choosing smaller increments and opting for longer computing time. Since we consider an uniform plasma flow along the field lines, our profiles do not have subpulse components.

Our model shows the effects such as the aberration and the retardation make the pulse profiles to become asymmetric about the pulse center. This phenomenon has been observed in most of the pulsar profiles, e.g., [22, 24].

In our model, we find if the sight line is at a fixed angle ( $\theta = -0.05^\circ$ , see, Fig. 5 b) to the particle trajectory plane, observer tends to receive a single sign circular polarization. This type of single sign circular polarization has been observed in many pulsars, e.g., [25].

## 6. Conclusions

By considering projected dipolar magnetic field lines on a plane perpendicular to the rotation axis, we have developed a 2D model for the particle dynamics in pulsar magnetosphere. The motive behind developing this model is to elucidate some of the rotational effects induced in the pulsar profiles. We have obtained the analytical expressions for the particle trajectory and its curvature

radius. The energy of particles increase at the expense of neutron star's rotational energy. We find the sight line orientation relative to the particle trajectory plane might determine the sign of circular polarization. The asymmetries observed in pulse profiles can be explained by considering the aberration-retardation effects.

**Appendix-A: To find a series expansion for the factor  $\hat{n} \times (\hat{n} \times \vec{\beta})$  that appears in Eq. (19)**

Consider  $\vec{\beta}$  in Cartesian co-ordinates:

$$\vec{\beta} = \frac{1}{c}(V_x \hat{x} + V_y \hat{y}), \quad (\text{A-1})$$

where  $\hat{x}$  and  $\hat{y}$  are the unit vectors along the  $x$  and  $y$ -axes, respectively, (Fig. 1). Then it follows from Eq. (2) that

$$V_x = V_r \cos\left(\frac{\phi_{\text{tot}}(t+t_0)}{2}\right) - V_\phi \sin\left(\frac{\phi_{\text{tot}}(t+t_0)}{2}\right), \quad (\text{A-2})$$

and

$$V_y = V_r \sin\left(\frac{\phi_{\text{tot}}(t+t_0)}{2}\right) + V_\phi \cos\left(\frac{\phi_{\text{tot}}(t+t_0)}{2}\right) \quad (\text{A-3})$$

Using Eq. (24), we derive the series expansions for radial velocity  $V_r$  and rotation velocity  $V_\phi$  :

$$V_r = \frac{dr}{dt}, \quad (\text{A-4})$$

$$V_\phi = r\Omega^*. \quad (\text{A-5})$$

By substituting  $V_r$  and  $V_\phi$  into by Eqs. (A-2) and (A-3), we obtain

$$\begin{aligned} V_x &= V_{x0} + V_{x1}t + V_{x2}t^2, \\ V_y &= V_{y0} + V_{y1}t + V_{y2}t^2 \dots \end{aligned} \quad (\text{A-6})$$

The expressions of  $V_{x0}$ ,  $V_{y0}$ ,  $V_{x1}$ ,  $V_{y1}$  ... in the above expansions are lengthy. Using the triple vector identity and the definitions of  $\hat{n}$ ,  $\hat{e}_{\parallel}$  and  $\hat{e}_{\perp}$ , we obtain

$$\hat{n} \times (\hat{n} \times \vec{\beta}) = -(\vec{\beta} \cdot \hat{e}_{\parallel}) \hat{e}_{\parallel} - (\vec{\beta} \cdot \hat{e}_{\perp}) \hat{e}_{\perp}, \quad (\text{A-7})$$

where

$$\vec{\beta} \cdot \hat{e}_{\parallel} = -\frac{\sin \theta}{c}(V_y \sin \eta + V_x \cos \eta), \quad (\text{A-8})$$

$$\vec{\beta} \cdot \hat{e}_{\perp} = \frac{1}{c}(V_y \cos \eta - V_x \sin \eta). \quad (\text{A-9})$$

Using the series expansions of  $V_x$  and  $V_y$ , we write

$$\hat{n} \times (\hat{n} \times \vec{\beta}) = \frac{1}{c} [\hat{e}_{\parallel} \sin \theta (V_{\parallel 0} + V_{\parallel 1}t + V_{\parallel 2}t^2) + \hat{e}_{\perp} (V_{\perp 0} + V_{\perp 1}t + V_{\perp 2}t^2)], \quad (\text{A-10})$$

where

$$V_{\parallel i} = V_{yi} \sin \eta + V_{xi} \cos \eta, \quad (\text{A-11})$$

$$V_{\perp i} = V_{xi} \sin \eta - V_{yi} \cos \eta, \quad (\text{A-12})$$

and  $i = 0, 1, 2$ .

### Appendix-B: Transformations for solving Eq. (19)

Using the method of Buschauer & Benford [20], we make the following transformations in order to solve the integral in Eq. (19).

Consider

$$\int_{-\infty}^{\infty} \exp[i(N_1 t + N_2 t^2 + N_3 t^3)] dt = \frac{1}{N_3^{1/3}} e^{iC_n} \int_{-\infty}^{\infty} \exp[i(z\tau + \tau^3)] d\tau, \quad (\text{B-1})$$

where

$$\tau = \frac{1}{N_3^{1/3}} \left( t + \frac{N_2}{3N_3} \right) \quad (\text{B-2})$$

is a dimensionless variable, and

$$z = \frac{1}{N_3^{1/3}} \left( N_1 - \frac{N_2^2}{3N_3} \right) \quad (\text{B-3})$$

By differentiating the Eq. (B-1) with respect to  $N_1$  and  $N_2$ , we obtain

$$\begin{aligned} \int_{-\infty}^{\infty} t \exp[i(N_1 t + N_2 t^2 + N_3 t^3)] dt &= \frac{1}{N_3^{2/3}} e^{iC_n} \left[ \int_{-\infty}^{\infty} \tau \exp[i(z\tau + \tau^3)] d\tau \right. \\ &\quad \left. - C_l \int_{-\infty}^{\infty} \exp[i(z\tau + \tau^3)] d\tau \right] \end{aligned} \quad (\text{B-4})$$

and

$$\begin{aligned} \int_{-\infty}^{\infty} t^2 \exp[i(N_1 t + N_2 t^2 + N_3 t^3)] dt &= \frac{1}{N_3^{1/3}} e^{iC_n} \left[ C_m \int_{-\infty}^{\infty} \exp[i(z\tau + \tau^3)] d\tau \right. \\ &\quad \left. + C_p \int_{-\infty}^{\infty} \tau \exp[i(z\tau + \tau^3)] d\tau \right]. \end{aligned} \quad (\text{B-5})$$

We define

$$L_1(z) = \int_{-\infty}^{\infty} \exp[i(z\tau + \tau^3)] d\tau = \frac{2}{3} \sqrt{z} K_{1/3}[2(z/3)^{3/2}], \quad (\text{B-6})$$

$$L_2(z) = \int_{-\infty}^{\infty} \tau \exp[i(z\tau + \tau^3)] d\tau = i \frac{2}{\sqrt{27}} z K_{2/3}[2(z/3)^{3/2}], \quad (\text{B-7})$$

$$B_0 = \frac{1}{N_3^{1/3}} e^{iC_n} L_1(z), \quad (\text{B-8})$$

$$B_1 = \frac{1}{N_3^{2/3}} e^{iC_n} [L_2(z) - C_l L_1(z)], \quad (\text{B-9})$$

$$B_2 = \frac{1}{N_3^{1/3}} e^{iC_n} [C_m L_1(z) - C_p L_2(z)], \quad (\text{B-10})$$

where

$$C_1 = \frac{N_2}{3N_3^{2/3}}, \quad (\text{B-11})$$

$$C_n = \frac{N_2}{3N_3} \left[ \frac{2N_2^2}{9N_3} - N_1 \right], \quad (\text{B-12})$$

$$C_m = \left[ \frac{2N_2^2}{9N_3^2} - \frac{N_1}{3N_3} \right], \quad (\text{B-13})$$

$$C_p = \frac{2N_2}{3N_3^{4/3}}. \quad (\text{B-14})$$

## References

- 1 Sturrock P A, *Astrophys. J.*, 164 (1971), 529.
- 2 Ruderman M, Sutherland P, *Astrophys. J.*, 196 (1975), 51.
- 3 Lyne A G, Manchester R N, *Mon. Not. Roy. Astr. Soc.*, 234 (1988), 477.
- 4 Karpman V I, Norman C A, ter Haar D, Tsitovich V N, *Phys. Scr.*, 11 (1975), 271.
- 5 Buschauer R, Benford G, *Mon. Not. Roy. Astr. Soc.*, 178 (1977), 189.
- 6 Stinebring D R, Cordes J M, Rankin J M, Wiesberg J M, Boriakoff V, *Astrophys. J. Sup.*, 55 (1984), 247.
- 7 Gangadhara R T, *Astron. Astrophys.*, 327 (1997), 155.
- 8 Gil J A, Lyubarsky Y, Melikidze G I, *Astrophys. J.*, 600 (2004), 872.
- 9 Machabeli G Z, Rogava A D, *Phy. Rev. A*, 50 (1994), 98.
- 10 Gangadhara R T, Lesch H, 1997, *Astron. Astrophys. Lett.*, 323 (1997), 45.
- 11 Rieger F M, Mannheim K, *Astron. Astrophys.*, 353 (2000), 473.
- 12 Gold T, *Nature*, 221 (1969), 25.
- 13 Blaskiewicz M, Cordes J M, Wasserman I, *Astrophys. J.*, 370 (1991), 643
- 14 Hibschan J A, Arons J, *Astrophys. J.*, 546 (2001), 382.
- 15 Peyman A, Gangadhara R T, *Astrophys. J.*, 566 (2002), 365.
- 16 Gangadhara R T, *Astron. Astrophys.*, 314 (1996), 853.
- 17 Pearson C E, *Hand Book of Applied Mathematics*, (1974) Van Nostrand Rienhold Company, 372.
- 18 Gangadhara R T, *Astrophys. J.*, 609 (2004), 335.
- 19 Jackson J D, *Classical Electrodynamics*, (1972) Wiley, N Y.
- 20 Buschauer R, Benford G, *Mon. Not. Roy. Astr. Soc.*, 177 (1976), 109.
- 21 Phillips J A, *Astrophys. J.*, 385 (1992), 282.
- 22 Gupta Y, Gangadhara R T, *Astrophys. J.*, 584 (2003), 418.
- 23 Rogava A D, Dalakishvili G, Osmanov Z, *Gen. Rel. Grav.*, 35 (2003), 1133.
- 24 Gangadhara R T, Gupta Y, *Astrophys. J.*, 555 (2001), 31.
- 25 Han J L, Manchester R N, Xu R X, Qiao G J, *Mon. Not. Roy. Astr. Soc.*, 300 (1998), 373.

Received : November 23, 2004      Revised : December 21, 2004      Accepted : December 23, 2004